AD

Technical Report DEVCOMAC-BLTR-24008

Summary of Analysis to predict Laser Induced Crack Initiation using the Extended Finite Element Method

Zackary Carpenter
Michael Macri
Greg Vigilante

U.S. Army Combat Capabilities Development Command
Armaments Center
Weapons and Software Engineering Center
Benét Laboratories
Watervliet, NY 12189

2024 March 26

The views, opinions, and/or findings contained in this report are those of the author(s) and should not be construed as an official Department of the Army position, policy, or decision, unless so designated by other documentation.

The citation in this report of the names of commercial firms or commercially available products or services does not constitute official endorsement by or approval of the U.S. Government.

REPORT DOCUMENTATION PAGE

Form Approved
OMB No. 0704-0188

1. REPORT DATE *(DD-MM-YYYY)*	2. REPORT TYPE	3. DATES COVERED *(From - To)*
03/26/2024	Technical Report	

4. TITLE AND SUBTITLE
Summary of Analysis to Predict Laser Induced Crack Initiation Using the Extended Finite Element Method

5a. CONTRACT NUMBER

5b. GRANT NUMBER

5c. PROGRAM ELEMENT NUMBER

6. AUTHOR(S)
Zackary Carpenter
Michael Macri
Greg Vigilante

5d. PROJECT NUMBER

5e. TASK NUMBER

5f. WORK UNIT NUMBER

7. PERFORMING ORGANIZATION NAME(S) AND ADDRESS(ES)
U.S. Army Combat Capabilities Development Command Armaments Center
Weapons and Software Engineering Center, Benét Laboratories Directorate
1 Buffington Street, Watervliet, NY 12189

8. PERFORMING ORGANIZATION REPORT NUMBER
DEVCOMAC-BLTR-24009

9. SPONSORING/MONITORING AGENCY NAME(S) AND ADDRESS(ES)

10. SPONSOR/MONITOR'S ACRONYM(S)

11. SPONSOR/MONITOR'S REPORT NUMBER(S)

12. DISTRIBUTION/AVAILABILITY STATEMENT
DISTRIBUTION STATEMENT A. Approved for public release; distribution is unlimited.

13. SUPPLEMENTARY NOTES

14. ABSTRACT
With the use of controllable-pulse-shape pulsed laser heating (PLH), we can induce thermal cracks in a systematic way, in a small area, with a large number of repetitions, that gives us the ability to generate a large statistical population of data that will isolate the conditions in which cracks arise. After which metallography is performed, allowing us to visualize the entire crack pattern induced by the laser. From this test data, we have analyzed how adjusting extended finite element material properties and mesh density to predict the crack initiation and stress response The results from the physical test data showed large spread of crack depths that were independent of the number of pulses. This corresponded with the finite elem

15. SUBJECT TERMS
FEA, XFEM, LPH, Tungsten

16. SECURITY CLASSIFICATION OF:			17. LIMITATION OF ABSTRACT	18. NUMBER OF PAGES	19a. NAME OF RESPONSIBLE PERSON
a. REPORT	b. ABSTRACT	c. THIS PAGE			Zackary Carpenter
					19b. TELEPHONE NUMBER *(Include area code)*
U/L	SAR	SAR	SAR	16	(520) 673-6077

INSTRUCTIONS FOR COMPLETING SF 298

1. REPORT DATE. Full publication date, including day, month, if available. Must cite at least the year and be Year 2000 compliant, e.g. 30-06-1998; xx-06-1998; xx-xx-1998.

2. REPORT TYPE. State the type of report, such as final, technical, interim, memorandum, master's thesis, progress, quarterly, research, special, group study, etc.

3. DATE COVERED. Indicate the time during which the work was performed and the report was written, e.g., Jun 1997 - Jun 1998; 1-10 Jun 1996; May - Nov 1998; Nov 1998.

4. TITLE. Enter title and subtitle with volume number and part number, if applicable. On classified documents, enter the title classification in parentheses.

5a. CONTRACT NUMBER. Enter all contract numbers as they appear in the report, e.g. F33315-86-C-5169.

5b. GRANT NUMBER. Enter all grant numbers as they appear in the report. e.g. AFOSR-82-1234.

5c. PROGRAM ELEMENT NUMBER. Enter all program element numbers as they appear in the report, e.g. 61101A.

5e. TASK NUMBER. Enter all task numbers as they appear in the report, e.g. 05; RF0330201; T4112.

5f. WORK UNIT NUMBER. Enter all work unit numbers as they appear in the report, e.g. 001; AFAPL30480105.

6. AUTHOR(S). Enter name(s) of person(s) responsible for writing the report, performing the research, or credited with the content of the report. The form of entry is the last name, first name, middle initial, and additional qualifiers separated by commas, e.g. Smith, Richard, J, Jr.

7. PERFORMING ORGANIZATION NAME(S) AND ADDRESS(ES). Self-explanatory.

8. PERFORMING ORGANIZATION REPORT NUMBER. Enter all unique alphanumeric report numbers assigned by the performing organization, e.g. BRL-1234; AFWL-TR-85-4017-Vol-21-PT-2.

9. SPONSORING/MONITORING AGENCY NAME(S) AND ADDRESS(ES). Enter the name and address of the organization(s) financially responsible for and monitoring the work.

10. SPONSOR/MONITOR'S ACRONYM(S). Enter, if available, e.g. BRL, ARDEC, NADC.

11. SPONSOR/MONITOR'S REPORT NUMBER(S). Enter report number as assigned by the sponsoring/ monitoring agency, if available, e.g. BRL-TR-829; -215.

12. DISTRIBUTION/AVAILABILITY STATEMENT. Use agency-mandated availability statements to indicate the public availability or distribution limitations of the report. If additional limitations/ restrictions or special markings are indicated, follow agency authorization procedures, e.g. RD/FRD, PROPIN, ITAR, etc. Include copyright information.

13. SUPPLEMENTARY NOTES. Enter information not included elsewhere such as: prepared in cooperation with; translation of; report supersedes; old edition number, etc.

14. ABSTRACT. A brief (approximately 200 words) factual summary of the most significant information.

15. SUBJECT TERMS. Key words or phrases identifying major concepts in the report.

16. SECURITY CLASSIFICATION. Enter security classification in accordance with security classification regulations, e.g. U, C, S, etc. If this form contains classified information, stamp classification level on the top and bottom of this page.

17. LIMITATION OF ABSTRACT. This block must be completed to assign a distribution limitation to the abstract. Enter UU (Unclassified Unlimited) or SAR (Same as Report). An entry in this block is necessary if the abstract is to be limited.

ABSTRACT

With the use of controllable-pulse-shape pulsed laser heating (PLH), we can induce thermal cracks in a systematic way, in a small area, with a large number of repetitions, that gives us the ability to generate a large statistical population of data that will isolate the conditions in which cracks arise. After which metallography is performed, allowing us to visualize the entire crack pattern induced by the laser. From this test data, we have analyzed how adjusting extended finite element material properties and mesh density to predict the crack initiation and stress response The results from the physical test data showed large spread of crack depths that were independent of the number of pulses. This corresponded with the finite element results showing the crack propagated in the first few pulses and then stayed at that depth for the remaining pulses. We observed comparable crack depths and crack quantities under the pulse in both the physical and FEA simulations.

Table of Contents

List of Figures

List of Tables

INTRODUCTION /BACKGROUND

Understanding fatigue processes is of vital importance for operator safety. In the Army context, it is imperative to know how many rounds a weapon system can safely fire before it will break, so that the system will be condemned well before this failure occurs. Similar considerations apply to industrial equipment. As a result, the fatigue process is well-studied, and can be thought of as consisting of two phases. In the first, a crack forms, and in the second, the crack propagates, links up with other cracks, and generally grows until eventually it extends through the entire component, leading to failure. The crack propagation process is well understood and proceeds in a predictable way once a crack initiates. Thus, for most service life tests, the input criterion requires that the part already contains some representative cracks; if this is not the case, there will be considerable scatter in the number of cycles to failure.

The reason for this is that the formation of cracks is a stochastic process that is poorly understood. This state of affairs is understandable. Cracks arise from service conditions that are difficult to isolate with precision, and studying cracks requires detailed and costly postmortem analysis that consumes otherwise usable (and sometimes expensive) parts. Moreover, the operation of the part so as to induce the crack formation is not always quick or inexpensive.

With the use of controllable-pulse-shape pulsed laser heating (PLH), we can induce thermal cracks in a systematic way, in a small area, with a large number of repetitions, that gives us the ability to generate a large statistical population of data that will isolate the conditions in which cracks arise. After which metallography is performed, allowing us to visualize the entire crack pattern induced by the laser. From this study, we have analyzed how adjusting extended finite element material properties mesh composition to predict the crack initiation and stress response.

For modeling the crack, the extended finite element method (XFEM) approach is used, which allows the crack to initiate and propagate independently of the mesh. There are several variants to the XFEM approach. The approach we are using is based on a concept of using phantom nodes. This approach is similar to cohesive elements.

EXPERIMENTAL TESTING

(U) A conventional square laser pulse is applied to the surface of a specimen resulting in linear temperature increase and an exponential decay resulting in crack formation within the material.

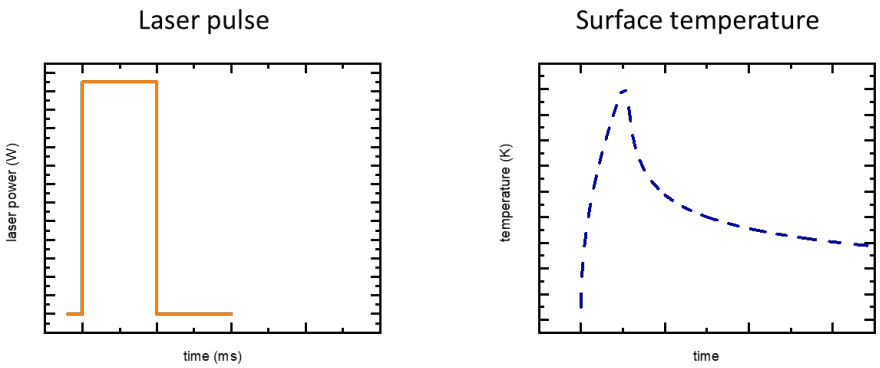

Figure 1: Laser pulse and surface temperature response

Testing was performed on a Tungsten W disk. The disk was 2 inch in diameter and 0.265 inches thick. The pulse laser heating, PLH, was performed using 5, 10, 25 and 50 pulse per spot at power levels of 0.8 and 1.0 J/mm with a 3mm diameter laser pulse. After the tests were completed, cross sectional metallography was performed to evaluate cracking.

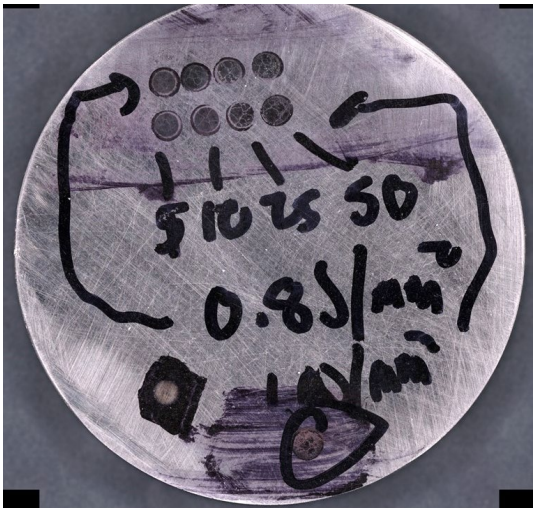

Figure 2: Tungsten test specimen

After sectioning, the sample was imaged to determine the extent of the grinding needed to evaluate cracking near the center of the pulse for each case.

Table 1: 0.8J/mm^2 sample grinding

	Sample	AVE Original Distance to Center of Pulse [mm]	[mils]	[in]	
	0.8 J/mm^2	1.60175	63.1	0.0631	
Comments	**Grinding Step**	**Mount Sample Thickness**	**Goal**	**Removed [in.]**	**Remaining [in.]**
	0	0.7630	0.6999	0.0000	0.0631
set to remove 20 and removed 14	1	0.7487		0.0143	0.0488
Set to remove 20 and removed 19	2	0.73		0.0187	0.0301
set to remove 26 and removed 27	3	0.703		0.0270	0.0031

Table 2: 1J/mm^2 sample grinding

	Sample	AVE Original Distance to Center of Pulse [mm]	[mils]	[in]	
	1.0 J/mm^2	1.08975	42.9	0.0429	
Comments	**Grinding Step**	**Mount Sample Thickness**	**Goal**	**Removed [in.]**	**Remaining [in.]**
	0	0.6979	0.6550	0.0000	0.0429
set to remove 20 and removed 17	1	0.6805		0.0174	0.0255
set to 20 and removed 20	2	0.6605		0.0200	0.0055

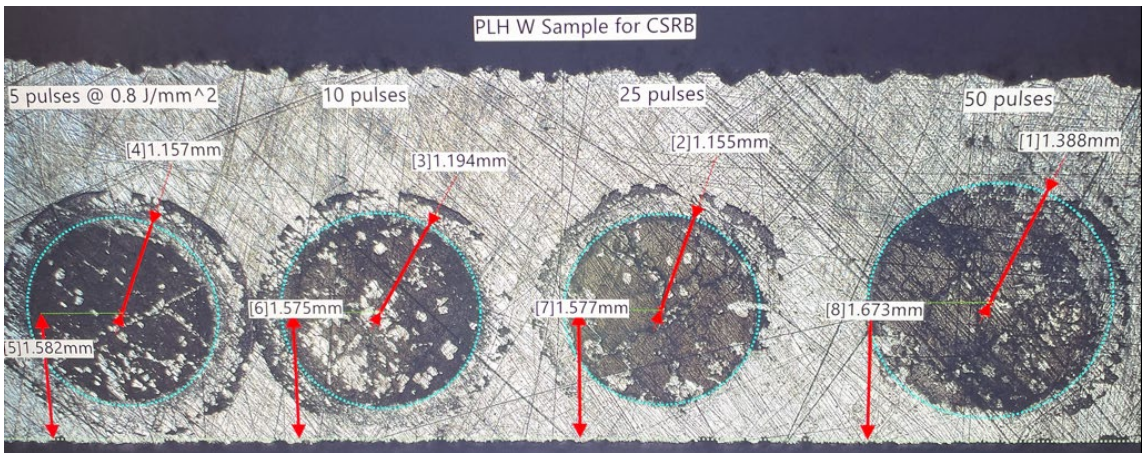

Figure 3: 0.8 J/mm^2 Samples

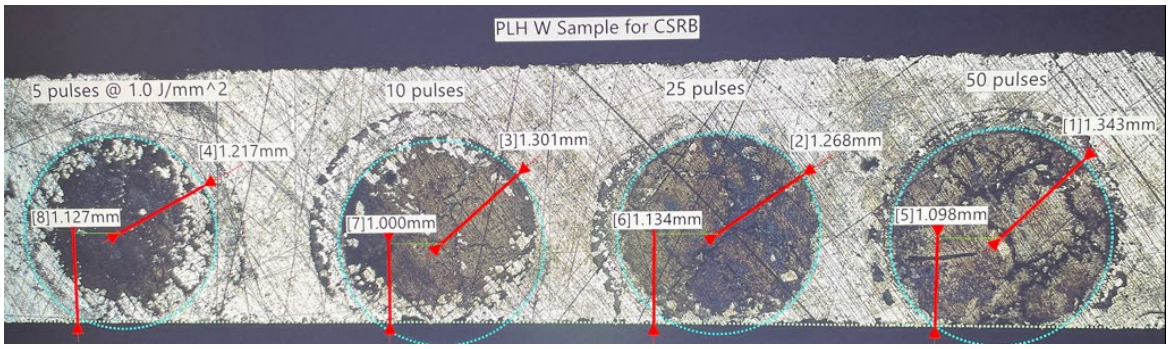

Figure 4: 1 J/mm^2 Samples

Figures 5-8 shows the cross-section crack response at different 0.8 J/mm^2 pulse loads. Figures 9-12 shows the cross-section crack response at different 1.0 J/mm^2 pulse loads. We note that in Figure 6 and 10 the ten pulse samples both had cracks through the entire specimen. Tables 3 and 4 summarize the data. We note that the 0.8J/mm^2 pulse generated 6 cracks on average, while the more intense 1.0J/mm^2 pulse averaged 5 cracks. Figure 13 shows a plot of the summarized data, ignoring the outlier data from the 10 pulse case. Several observations from Figure 13. First, we note that neither pulse loads produced increasing crack lengths as the number of pulses increased. Only the largest crack for the 1.0J/mm^2 case showed this. In fact, in examining the images and summary data, we note a large spread of the data. We believe this is due the brittleness of Tungsten, and that future testing should be performed on a more elastic specimen to calibration testing. For purposes of this study, we have chosen to focus on the 0.8J/mm^2 cases.

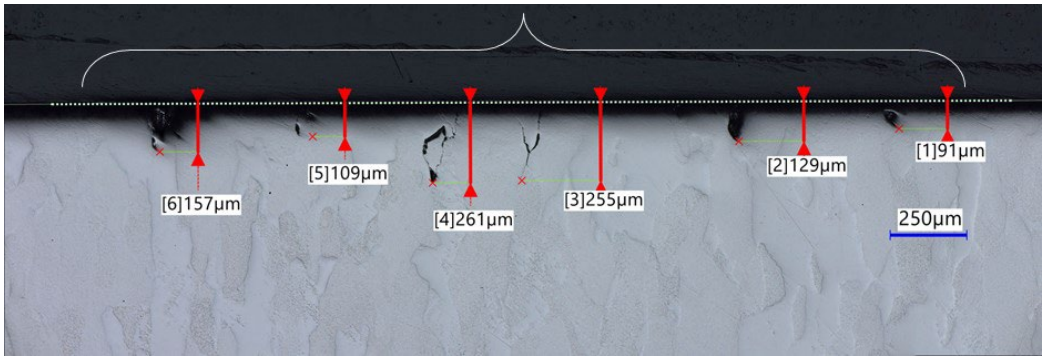

Figure 5: 0.8J/mm^2, 5 pulses

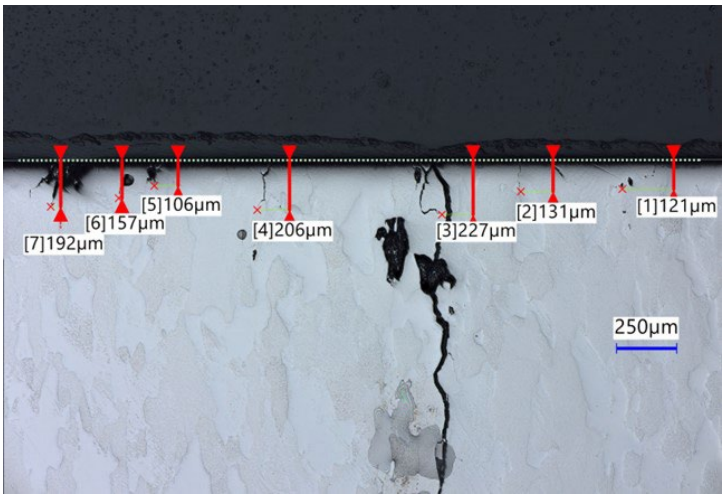

Figure 6: 0.8J/mm^2, 10 pulses

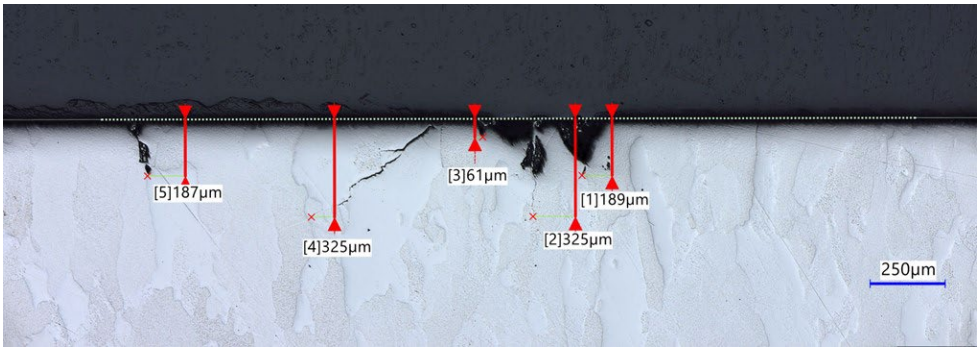

Figure 7: 0.8J/mm^2, 25 pulses

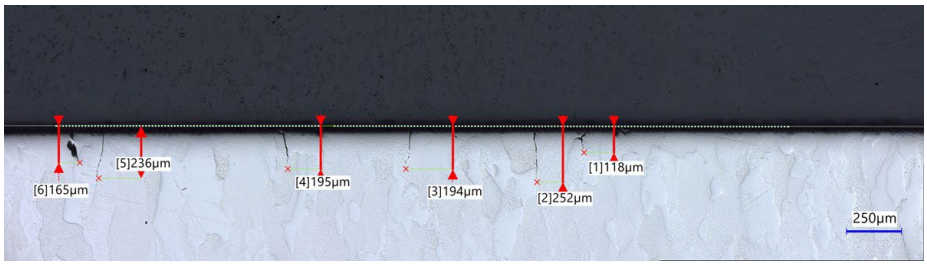

Figure 8: 0.8J/mm^2, 50 pulses

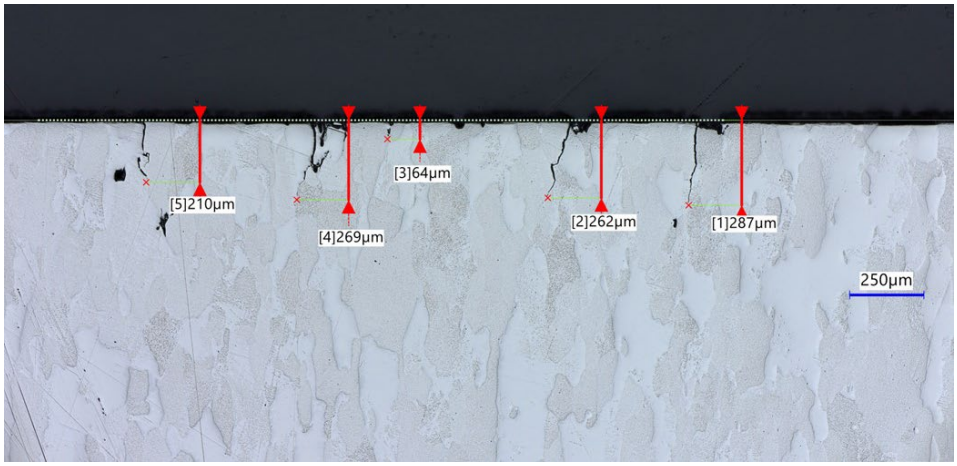

Figure 9: 1J/mm^2, 5 pulses

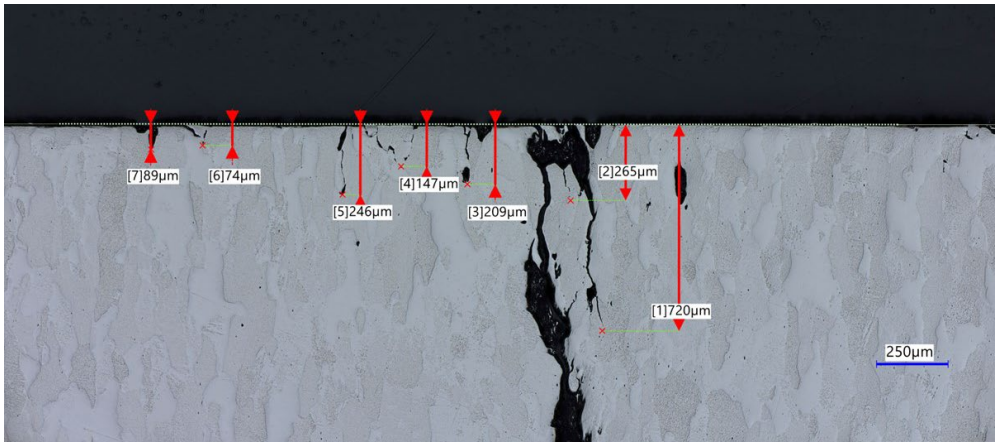

Figure 10: 1J/mm^2, 10 pulses

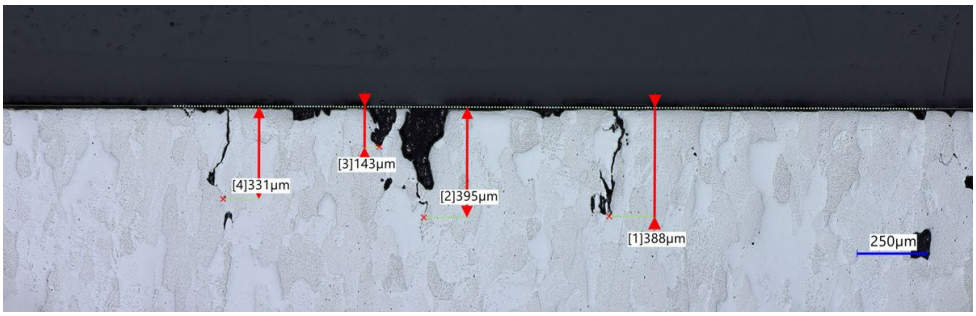

Figure 11: 1J/mm^2, 25 pulses

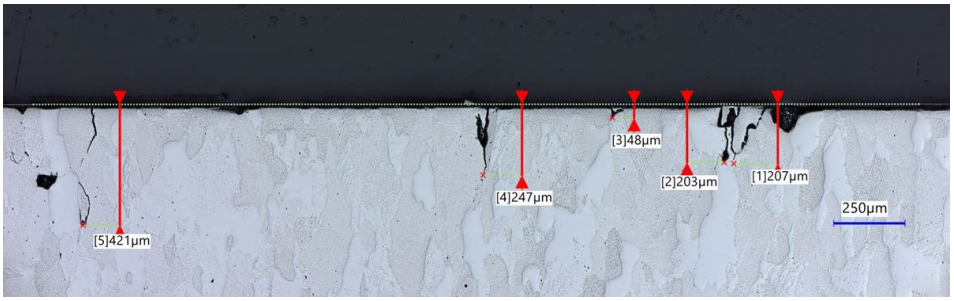

Figure 12: 1J/mm^2, 50 pulses

Table 3: Summary of 0.8J/mm2 Data

	5 pulses	10 pulses	25 pulses	50 pulses
# cracks	6	8	5	6
shortest crack (microns)	91	106	61	118
deepest crack (microns)	261	6731	325	252
AVE	167	984	217	193

Table 4: Summary of J/mm2 Data

	5 pulses	10 pulses	25 pulses	50 pulses
# cracks	5	8	4	5
shortest crack (microns)	64	74	143	48
deepest crack (microns)	287	6731	395	421
AVE	218	1060	314	225

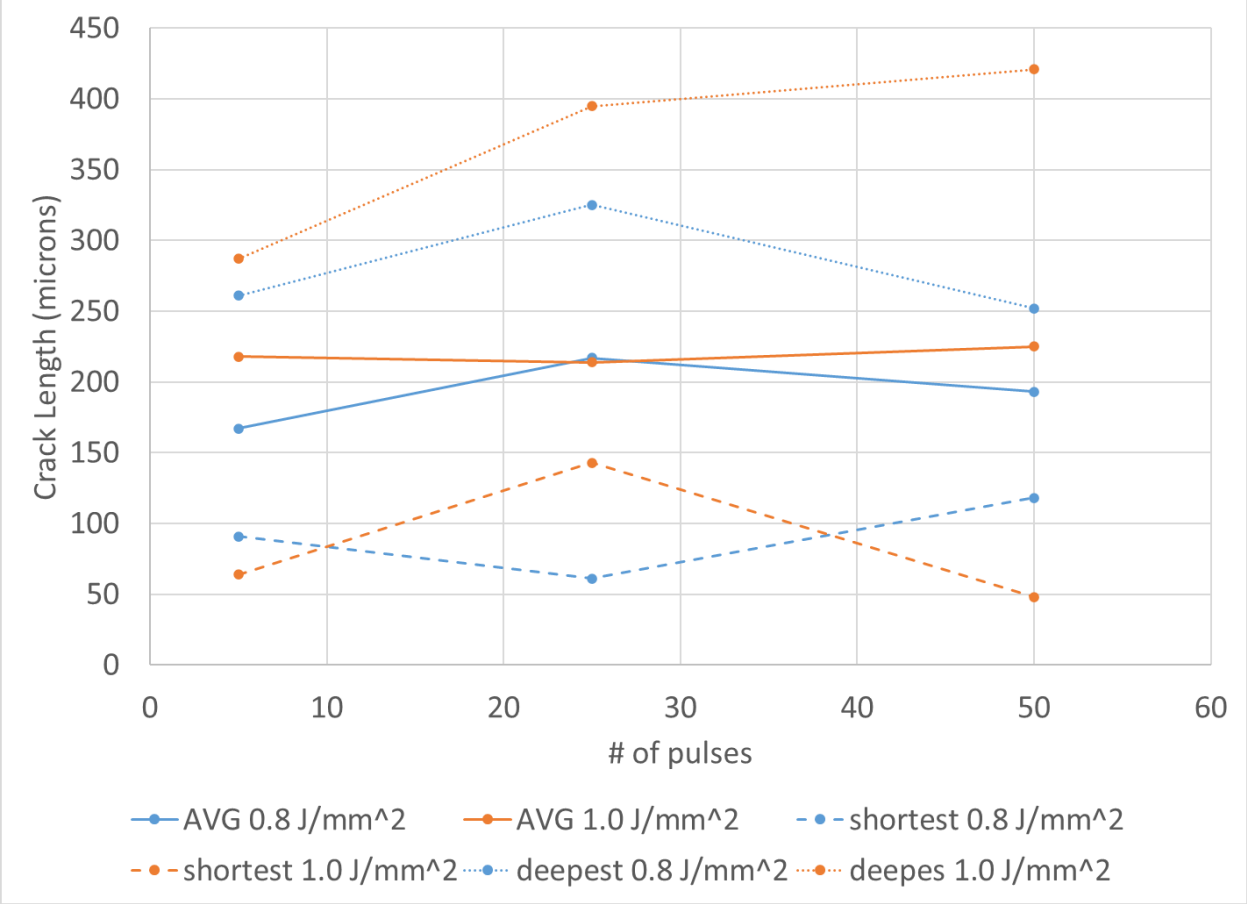

Figure 13: Plot summary of data

NUMERICAL ANALYSIS

The XFEM approach is used to capture crack initiation. There are several variants to the XFEM approach. Within the XFEM framework, cracks can initiate and propagate independently of the mesh.

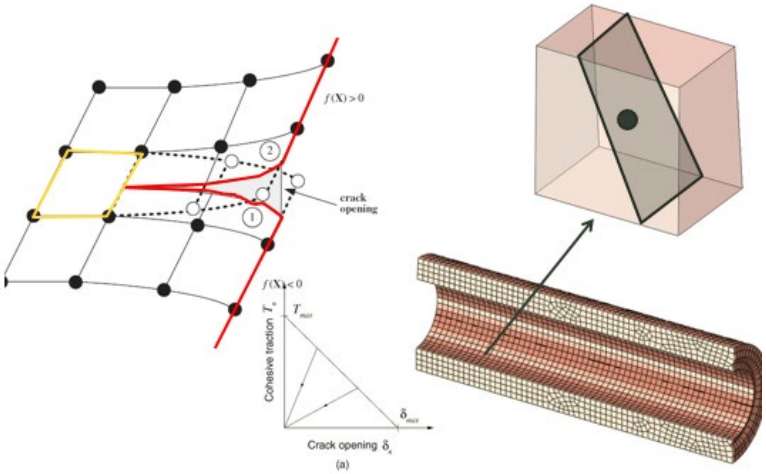

Figure 14: XFEM Crack Initiation

In XFEM, each element in a designated region is examined at the centroid for a trigger criterion such as a critical stress or strain. For this work we examined using a critical maximum principal stress as the critical criteria, $\sigma_{critical}$. This unknown value is material dependent will be evaluated with the test data to determine the value. To determine $\sigma_{critical}$, finite element analysis (FEA) simulations were performed varying the value of $\sigma_{critical}$ up to the ultimate tensile strength (UTS). The results are compared with the physical test data to calibrate $\sigma_{critical}$ to predict crack initiation at the correct loading conditions. With each time/load iteration in the FEA simulation the calculated maximum principal stresses are compared with the $\sigma_{critical}$.

Once the maximum principal stress exceeds this value the XFEM algorithms are activated with the code. The calculation of the displacement for degrees on freedom on the replaced with

$$u^h = \sum_{I \in n} N_I(\boldsymbol{x}) \left[u_I + H(\boldsymbol{x}) a_I + \sum_{\alpha=1}^{\xi} F_\alpha(x) b_I^\alpha \right] \quad (1)$$

(U) Where N_I is a standard finite element shape function, dependent on the element type chosen. u_I are the standard unknown degrees of freedom that are solved for to determine the resulting displacements. $H(x)$ is a Heaviside Function and used to separate the element by the crack which resides on $\mathrm{H}(0)$. The F_α functions are used to capture the stress field around the crack tip. a_I and b_I are additional degrees of freedom needed to capture the additional functions in the stress field.

(U) Abaqus software is used for implementing finite elements. Abaqus uses a variation of the XFEM approach using what has been termed phantom nodes. In this process, once

the crack is detected, it splits the element such that the split is on a plane perpendicular to max principal stress. In the phantom XFEM approach the term, $H(x)a_I$, is adapted as additional "phantom" nodes, as shown in figure 16. These nodes in effect replace the XFEM element with a cohesive like set of elements.

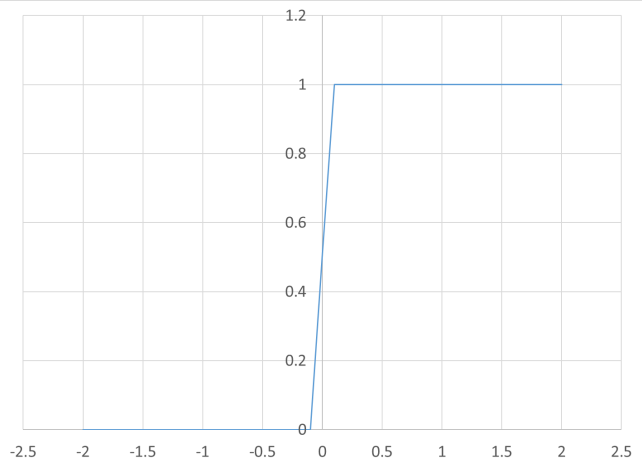

Figure 15: Heaviside function

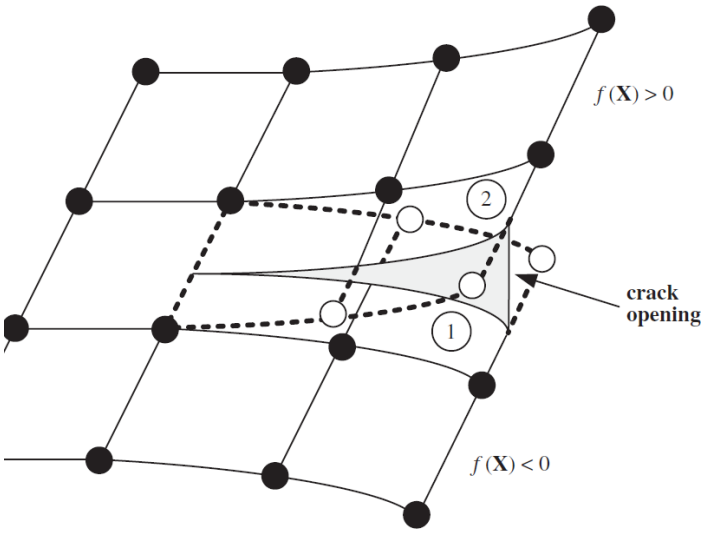

Figure 16: Phantom Node Approach

The crack tip functions, $\sum_{\alpha=1}^{\xi} F_\alpha(x) b_I^\alpha$, are accounted for in the cohesive properties. Complete separation of the element does not occur at this point, as is would in a standard XFEM approach. The element slowly degrades as the crack opens. This represents the plastic zone in the material and well as the region around the crack. The damage, D, is related to the traction – crack opening graph, shown in figure 17. Thus, the crack tip resides somewhere in the final damaged element and not necessarily at the shown tip

$$D = \frac{\delta^f(\delta^{max} - \delta^0)}{\delta^{max}(\delta^f - \delta^0)} \quad (2)$$

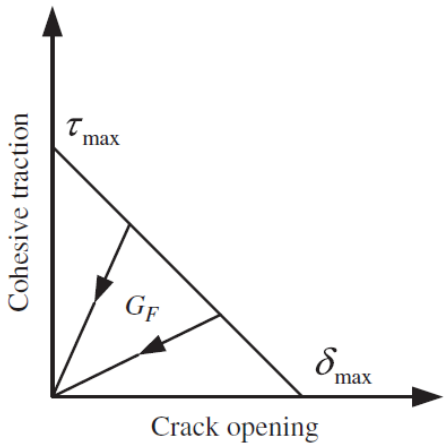

Figure 17: Damage vs crack opening

In function (2), δ^0 is the initial crack opening, δ^{max} is the maximum opening at failure. δ^f is the current opening and G_F the Fracture energy. D is then used in the stress-strain relationship such that

$$\sigma_{ij} = (1 - D)C_{ijkl}\varepsilon_{kl} \quad (3)$$

For the FEA simulation a two dimensional (2D) cross section of the region around a laser pulse was modeled as shown in Figure 18. The boundary conditions are shown in Figure 19. The side and bottom represent the rest of the wafer. The Flux pulse over a 3mm edge represents the 0.8J/mm^2 pulse.

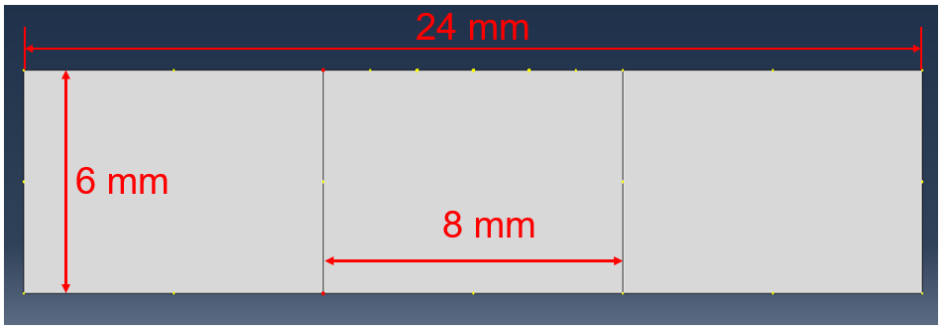

Figure 18: FEA part model

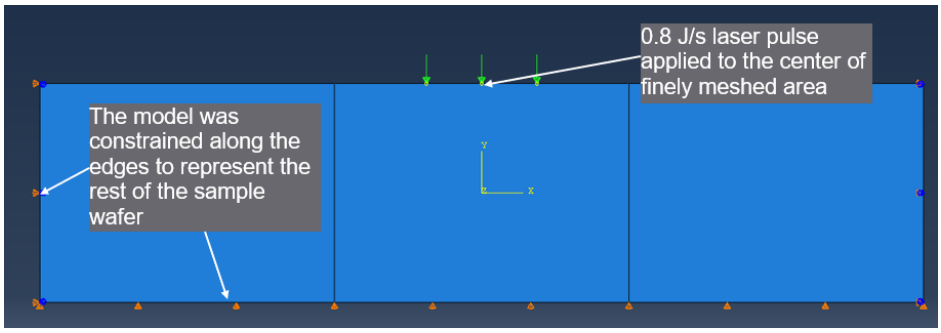

Figure 19: FEA boundary conditions

The pulse is applied as a flux square wave with a magnitude of 385×10^3 over a 0.0026s time frame to produce the surface temperature response as seen in figure 1. This is equivalent to a 1.0J/mm^2 pulse. The properties used for Tungsten are:

Table 5: Tungsten Material Properties

Property	Value
Conductivity	W/m/K K 163 300 146 473.15 128 873.15 117 1273.15
Density	1.93E-08 Tonne/mm^3
Young's Modulus	MPa K 400000 300 370000 1073.15 350000 1473.15 300000 2073.15
Poisson's Ratio	0.28
Yield Stress	750 MPa
UTS	862.5 MPa
Thermal Expansion	4.6E-06 K^-1
Specific Heat	1.34e8 mJ/tonne/K

We examined several case studies, varying the $\sigma_{critical}$ and the mesh refinement around the region. The first highlighted case is shown in Figure 20. The mesh generated was 50 microns by 100 microns elements. The $\sigma_{critical}$ is set to 700MPa. The results show a fairly uniform stress field under the laser with a 150 micron crack forming after the first pulse and staying at that depth through 50 pulses. In the second case we increase the $\sigma_{critical}$ to 800MPa. This showed the crack depth reducing to 50 microns after the first pulse, expanding to 100 microns after the second pulse and staying at 100 microns after the second pulse, as shown in figure 21. In case 3, shown in figure 22, we induced the mesh

to 150 microns x 150 microns and reduced the $\sigma_{critical}$ to 300MPa. The results show an increase to a 450 micron crack forming after the first pulse and not propagating further.

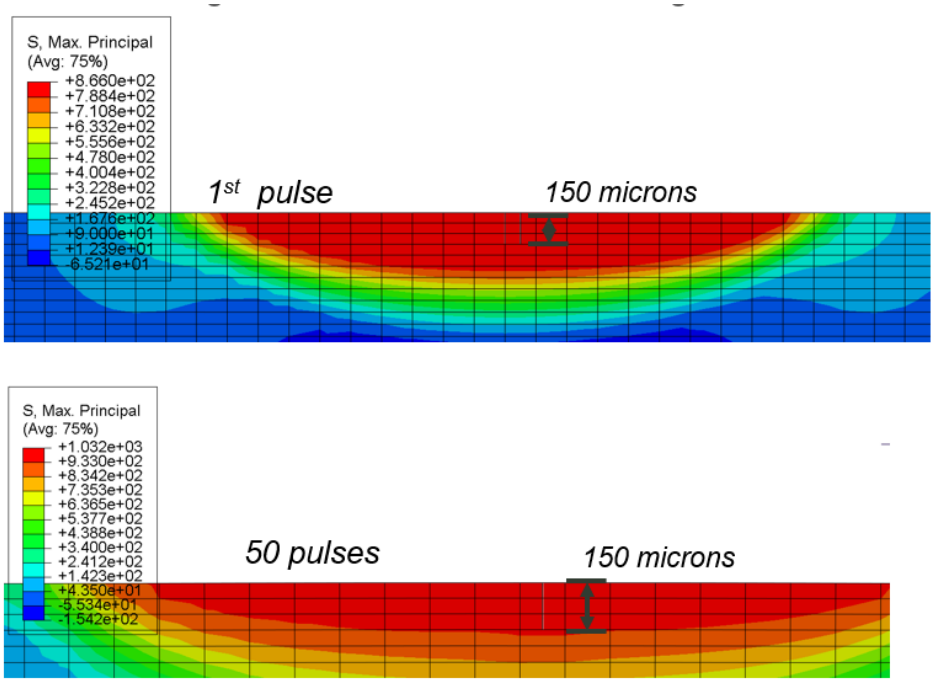

Figure 20: Case 1: 50x100 micron elements with 700MPa damage criteria

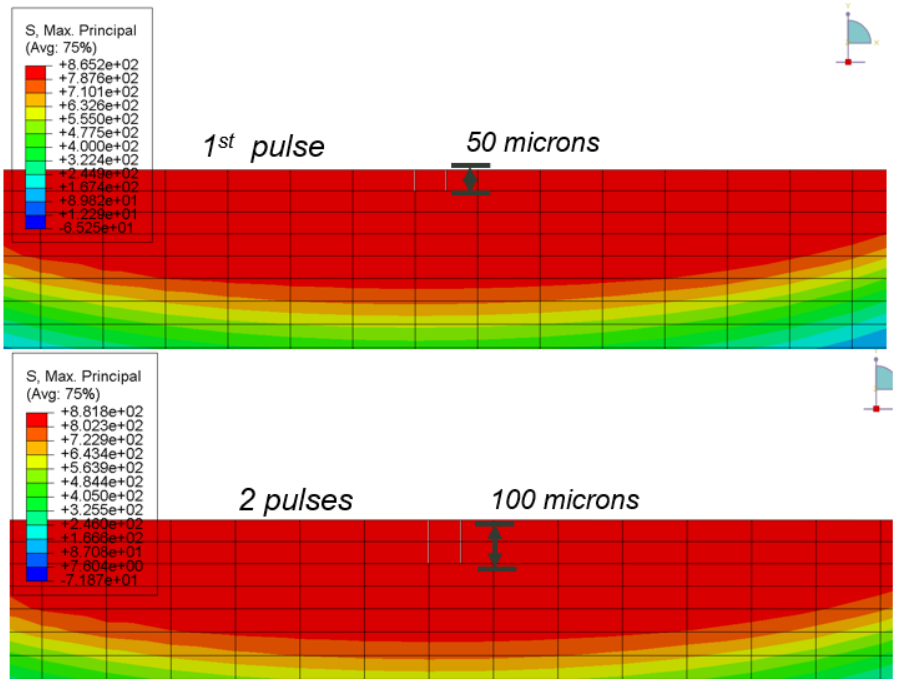

Figure 21: Case 2: 50x100 micron elements with 800MPa damage criteria

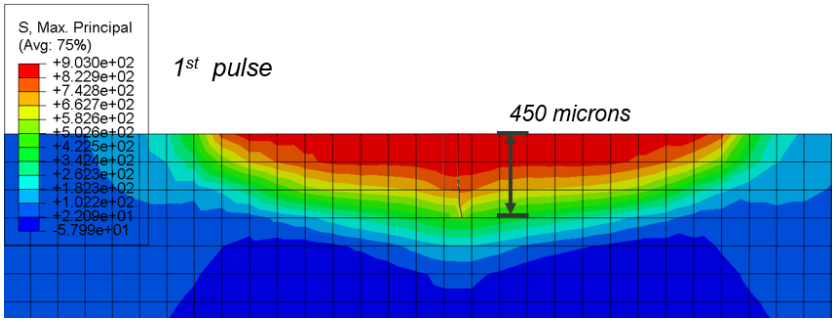

Figure 22: Case 3: 150x150 micron elements with 300MPa damage criteria

For case four we refined the mesh such that the elements were 20 microns deep and 15 microns wide, shown in Figure 23. The $\sigma_{critical}$ was calibrated to 300 MPa. This resulted in 31 cracks created down to 200 microns. Results are shown in Figure 24. The cracks form very close together and appear dependent of the mesh. In Figure 25 the mesh was updated to 80 microns deep and 160 microns wide. The results show 3 cracks at 160 microns deep. In case six we updated the mesh to 20 microns deep and 200 microns wide and 20 microns deep. The results are shown in Figure 26, showing 6 cracks at 180 microns deep. Examining Figures 24-26 we see cracks depths within range of what was seen in the physical test data. We also see that the number of cracks generated appears dependent on the mesh. At close examination of the stress generated under the laser pulse is relatively constant, unlike a notched specimen where there is a stress concentration. This results in multiple elements on the surface under the laser triggering the crack initiation.

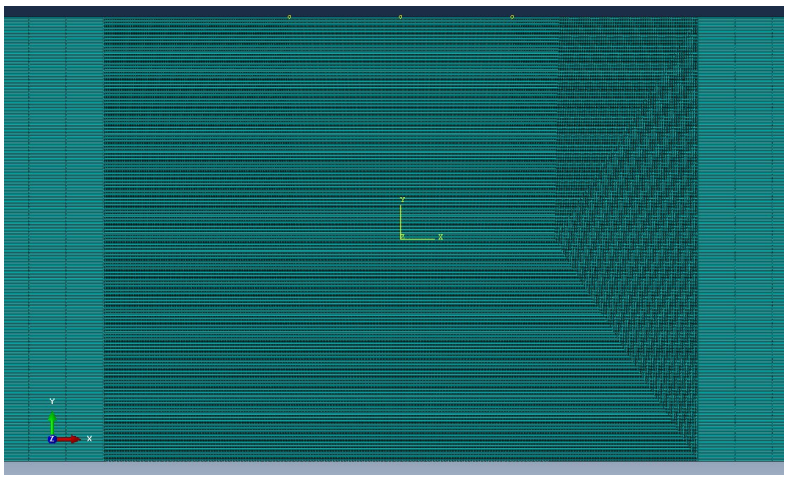

Figure 23: Mesh Refinement

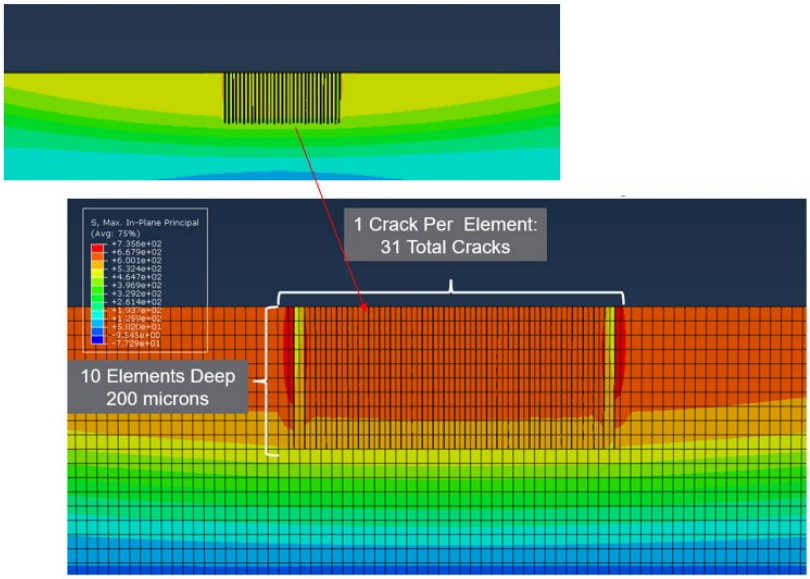

Figure 24: Case 1 20 microns x 15 microns elements

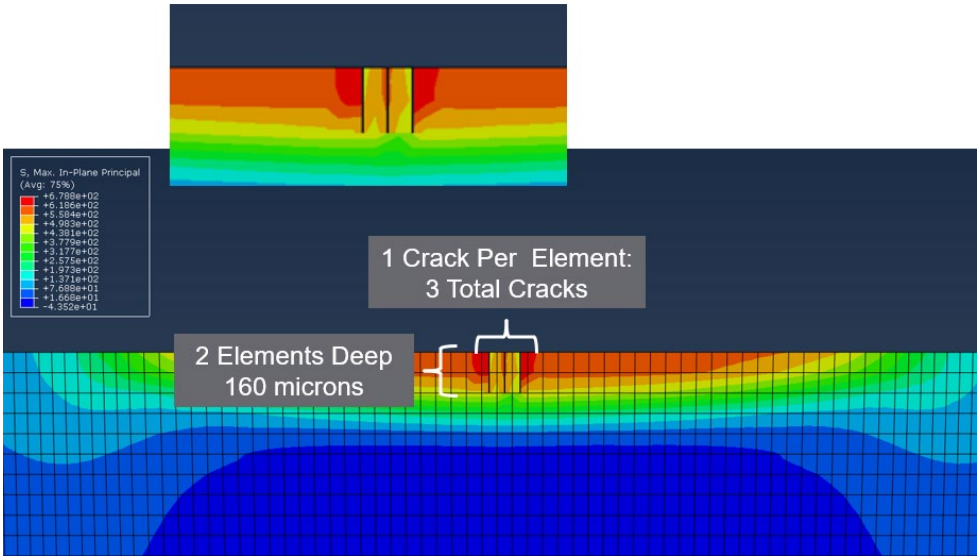

Figure 25: Case 2 80 microns x 160 microns elements

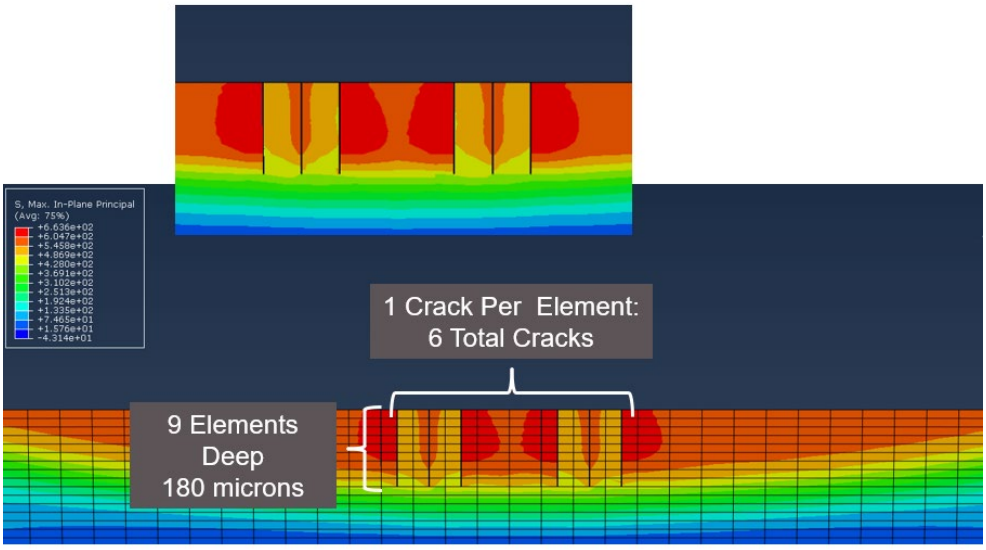

Figure 26: Case 3 20 microns x 200 microns elements

SUMMARY/CONCLUSIONS

With the use of controllable-pulse-shape pulsed laser heating (PLH), we can induce thermal cracks in a systematic way, in a small area, with a large number of repetitions, that gives us the ability to generate a large statistical population of data that will isolate the conditions in which cracks arise. After which metallography is performed, allowing us to visualize the entire crack pattern induced by the laser. From this test data, we have analyzed how adjusting extended finite element material properties mesh composition and mesh density to predict the crack initiation and stress response The results from the physical test data showed large spread of crack depths that were independent of the number of pulses. This corresponded with the finite element results showing the crack propagated in the first few pulses and then stayed at that depth for the remaining pulses. We observed a low critical stress criteria however, there is indication that it is mesh dependent. Future work should include further testing with more elastic material to see if the results can be repeated.

REFERENCES

1. Dolbow J. *An extended finite element method with discontinuous enrichment*. Northwestern University, 1999.
2. Cruse T. *Boundary element analysis in computational fracture mechanics*. Dordrecht: Kluwer; 1988.
3. Carter BJ, Wawrzynek PA, Ingraffea AR. Automated 3-D crack growth simulation. *Int. J. Num. Meth. Eng* 2000; 47:229–53.
4. Melenk JM, Babuska I. The partition of unity finite element method: basic theory and applications. *Comput Methods Appl Mech Engng* 1996; 139:289–314.
5. Song JN, Areias PM, Belytschko T. A method for dynamic crack and shear band propagation with phantom nodes. *Int. J. Numer. Meth. Engng* 2006; 67:868–893
6. Daux C, Moes N, Dolbow J, Sukumar N, Belytschko T. Arbitrary branched and intersecting cracks with the extended finite element method. Int. J. Numer. Meth. Engng 2000; 48:1741-1760
7. Chessa J, Wang H, Belytschko T. On the construction of blending elements for local partition of unity enriched finite elements. *Int. J. Num. Meth. Eng* 2003; 57:1015-1038.
8. Macri M, De S, Shephard M. Hierarchical Tree-Based Discretization for the Method of Finite Spheres. *Computers & Structures* 2003; 81:789-803
9. Stolarska M, Chopp DL, Moës N, Belytschko T. Modeling crack growth by level sets in the extended finite element method. International Journal for Numerical Methods in Engineering 2001; 51(8):943–960.